A. Distortions to local geometry

While characterizing the CTL of substitutional defects in diamond and 3C-SiC, we analyzed the distortions to local geometries of these defects at different charge states. These calculations show that the most stable ground state geometry for nitrogen is heavily dependant on its charge state. Positively charged nitrogen exhibits T_d symmetry, where all four neighboring N-C bonds are 1.56 Å in length, compared to the equilibrium C-C bond length of 1.55 Å. For neutral nitrogen however, this changes dramatically. In this case it is stabilized in C_{3v} symmetry, with one of the N-C bonds being elongated to 2.04 Å, a 33% change compared to the equilibrium C-C bond length observed in other studies previously [1]. The effect of charge is not as pronounced for boron and phosphorus. The only difference between the neutral and negatively charged state for boron comes from the fact that in the former there is a small Jahn-Teller distortion that elongates one of the B-C bonds [2]. The B-C equilibrium bond length is found to be 1.58 Å, while in the neutral case under the small Jahn-Teller distortion the elongated bond is 1.61 Å. This is consistent with previous experimental observations [3]. For phosphorus, there is no noticeable change between different charge states, and all four neighboring bond lengths for any state are 1.70 Å. The reason that the PBE and the HSE functionals give a very similar characterization of the CTL of B_C and P_C is that these defects are both relatively shallow defects in diamond. Consequently, their distortions to local geometries are not very pronounced and the PBE and HSE functionals both predict the same local geometry and the same bond lengths with the surrounding neighboring atoms.

The ground state geometry for the N_C donor in 3C-SiC does not show any sensitivity to the charge state of N_C. In both charge states, all four of the neighboring bond lengths are 1.92 Å. This is very similar to the P_C donor in diamond. In both cases, there is virtually no difference between the local geometries of the negatively charged and neutral charge states. However, for P_C in diamond, the neighboring bonds are elongated by 10% compared to the equilibrium bond length. This number is only 1% for N_C in 3C-SiC. The perturbation to the host's local geometry is more noticeable for P_C in diamond, which manifests as a considerably deeper donor in diamond compared to N_C in 3C-SiC. On the other hand, both Al_{Si} and B_C undergo a mild geometric distortion upon changing their charge state. Both defects show $C_{3v}(T_d)$ symmetry in their neutral (negative) charge state. In its neutral charge state, B_C has one elongated bond length at 2.04 Å and its three remaining neighboring bonds are 1.94 Å. While negatively charged, all four bonds remain at 1.92 Å. For Al_{Si}, the elongated bond at its neutral charge state sits at 2.03 Å and the three neighboring bonds are 1.98 Å. While negatively charged, all four bonds are 1.99 Å. The slightly more pronounced distortion that B_C undergoes compared to Al_{Si} while changing its charge state is also the reason why B_C is a deeper acceptor compared to Al_{Si}. Even though there are many shallow defects in diamond and SiC that could also work for forming DAPs with resolvable spectra, we provide here a small number of examples, with some deep and shallow defects to illustrate their differences. We acknowledge that there are many defect candidates that could work, and our list of examples is not meant to be an exhaustive one.

Supplementary Table 1: Local geometries of defects. Symmetries and ground state geometries of substitutional defects in diamond and 3C-SiC are given based on their respective charge states. Bond lengths are given in units of the calculated diamond equilibrium C-C bond length of 1.55 Å for defects in diamond. For defects in 3C-SiC, the respective equilibrium Si-C bond length of 1.90 Å is used. The numbers in brackets indicate the number of bonds of the given length stemming from each central atom.

Host	Defect	q	Symmetry	Bond length
Diamond	B_C	0	C_{3v}	1.02(3), 1.04(1)
		-1	T_d	1.02(4)
	N_C	0	C_{3v}	0.95(3), 1.33(1)
		1	T_d	1.01(4)
	P_C	0	T_d	1.10(4)
		1	T_d	1.10(4)
3C-SiC	B_C	0	C_{3v}	1.02(3), 1.08(1)
		-1	T_d	1.01(4)
	N_C	0	T_d	1.01(4)
		1	T_d	1.01(4)
	Al_{Si}	0	C_{3v}	1.04(3), 1.07(1)
		-1	T_d	1.05(4)

Supplementary Table 2: ZPL energies for DAPs. ZPL energies for all the DAP in diamond and SiC are reported in units of eV. Note that since both B and N replace C atoms in 3C-SiC, no nearest neighbors are possible. B-N pairs can only form even numbered shells. Similarly, Al-N pairs can only have odd numbered shells.

	B-N (diamond)		B-N (3C-SiC)		Al-N (3C-SiC)	
Shell #	PBE	HSE	PBE	HSE	PBE	HSE
m1	3.57	4.35	-	-	1.37	2.22
m2	3.14	3.88	1.21	1.79	-	-
m3	3.08	3.81	-	-	1.34	2.17
m4	2.98	3.70	1.16	1.69	-	-
m5	2.98	3.69	-	-	1.32	2.15
m6	2.91	3.63	1.13	1.66	-	-
m7	2.87	3.57	-	-	1.31	2.12
m8	2.87	3.57	1.12	1.64	-	-
m9	2.85	3.56	-	-	1.31	2.10
m10	2.84	3.55	1.10	1.62	-	-

Supplementary Table 3: Summary of parameters from the effective 1D-CC model. Calculated parameters for the effective one-dimensional model for DAP in 3C-SiC and diamond. ZPL energies and total mass-weighted distortion ΔQ are given as well as effective frequencies ($\Omega_{\{e,g\}}$) and HR factors ($S_{\{e,g\}}$) in ground and excited states.

DAP	ZPL (eV) PBE (HSE)	ΔQ (amu$^{1/2}$Å) PBE (HSE)	$\hbar\Omega_g$ (meV) PBE (HSE)	$\hbar\Omega_e$ (meV) PBE (HSE)	S_g PBE (HSE)	S_e PBE (HSE)
B-N (SiC) m2	1.21 (1.60)	0.521 (0.796)	60.35 (61.90)	46.72 (48.74)	1.96 (4.69)	1.52 (3.69)
B-N (SiC) m4	1.16 (1.51)	0.627 (0.854)	60.03 (61.50)	47.64 (51.18)	2.82 (5.36)	2.24 (4.46)
B-N (SiC) m6	1.13 (1.48)	0.578 (0.767)	63.13 (67.45)	50.49 (55.54)	2.53 (4.75)	2.02 (3.91)
B-N (SiC) m8	1.12 (1.47)	0.597 (0.781)	63.83 (67.83)	51.65 (56.37)	2.72 (4.96)	2.20 (4.12)
B-N (SiC) m10	1.10 (1.45)	0.601 (0.780)	63.63 (67.67)	51.47 (56.61)	2.75 (4.92)	2.23 (4.12)
Al-N (SiC) m1	1.37 (1.90)	0.111 (0.112)	75.29 (77.54)	74.52 (76.62)	0.11 (0.12)	0.11 (0.12)
Al-N (SiC) m3	1.34 (1.86)	0.170 (0.206)	70.84 (71.31)	66.28 (61.73)	0.25 (0.36)	0.23 (0.31)
Al-N (SiC) m5	1.32 (1.85)	0.198 (0.239)	65.37 (66.12)	60.73 (57.53)	0.31 (0.45)	0.28 (0.39)
Al-N (SiC) m7	1.31 (1.84)	0.213 (0.274)	63.91 (66.40)	57.99 (53.80)	0.35 (0.60)	0.31 (0.48)
Al-N (SiC) m9	1.31 (1.82)	0.222 (0.314)	66.10 (67.78)	59.34 (52.07)	0.39 (0.80)	0.35 (0.61)
B-N (diamond) m2	3.14 (3.88)	1.431 (1.498)	69.09 (70.77)	77.72 (84.97)	16.91 (19.00)	19.03 (22.82)
B-N (diamond) m5	2.98 (3.69)	1.439 (1.501)	68.74 (70.89)	78.80 (85.67)	17.02 (19.10)	19.51 (23.09)
B-N (diamond) m8	2.87 (3.57)	1.428 (1.472)	68.75 (71.31)	80.06 (87.52)	16.77 (18.48)	19.53 (22.68)
B-P (diamond) m2	3.97 (5.10)	0.184 (0.239)	92.60 (86.43)	90.20 (81.33)	0.37 (0.59)	0.37 (0.56)
B-P (diamond) m5	3.90 (5.00)	0.231 (0.420)	83.45 (70.08)	78.86 (57.73)	0.53 (1.48)	0.50 (1.22)
B-P (diamond) m8	3.83 (4.91)	0.252 (0.470)	80.61 (69.49)	76.87 (56.23)	0.61 (1.84)	0.58 (1.49)

B. Electric Dipole Moments

We obtain the electric dipole moments of DAPs using two different methods. First we obtain it by using MLWFs according to the Modern Theory of Polarization. The second method is by applying a homogeneous electric field to the supercell, observing the change in ZPL, and evaluating the instantaneous slope at zero field value, as is demonstrated in Figure 4. Supplementary Table 5 below shows how closely the results from the two methods agree with each other. In Figure 3, we also report a range of values for the electric dipole moments of various shells in diamond and SiC. This is because the specific geometric orientations of the donor's and the acceptor's distorted bonds in the crystal, not just the pair distance, have an effect on the final dipole moment observed. When the distorted bonds of the donor and acceptor face each other in the crystal, then the resulting dipole moment ends up less than eR_m; and When facing away from each other, the resulting dipole moment is greater than eR_m. In other cases, neither will be true, and the distorted bonds will be roughly parallel to each other. In these cases, the dipole moment will be very close to eR_m. In real experiments, we believe that this spontaneous dipole moment may not be measurable, and instead, an *average* would be obtained, since the choice of which of the four bonds gets distorted could vary from one excitation cycle to the next. In the end, this *average* should be very close eR_m. To corroborate this claim, we provide additional data points (red crosses in Figure 3) for a few select shells in diamond and SiC, and provide the relative orientations of the donor and acceptor in the crystal along with the resulting dipole moments in Supplementary Table 4. However, care must be taken not to confuse these orientations with the orientations of the distorted bonds of the donor and acceptor. Since the dipole stems from the nature of the charge transfer excitation, the resulting dipole moment will obviously depend on the donor and acceptor's orientations to each other, (i.e. the dipole can be approximated with eR_m) Still, the exact value of this dipole (whether it is greater than, less than, or close to eR_m) will be determined by the relative orientations of the distorted bonds in the vicinity of the donor and acceptor. This conclusion is also evident from a lack of correlation between dipole moments and the relative orientations of the donor and acceptor in the crystal, as seen in Supplementary Table 4.

C. Zero Phonon Lines & J($\mathbf{R_m}$) correction

As can be seen in Supplementary Table 2, the ZPL energies decrease with increasing shell number and inter-defect distance. This is in good qualitative agreement with what is expected. It is well known that the PBE functional often underestimates the ZPL energy [4]. Therefore, it is not surprising that the results obtained with the HSE functional have slightly more energy than those obtained using PBE. The results obtained for explicitly calculated $J(R_m)$ correction integrals are presented in Supplementary Figure 1. These integrals are calculated using KS orbitals corresponding to the hole and electron wavefunctions bound to acceptors and donors respectively. As expected, this correction term

Supplementary Table 4: Electric dipole moment dependence on DAP orientations in the crystal. Orientations of the donor atom with respect to the acceptor atom in the supercell in units of the lattice constant a_0 and the resulting dipole moment from a MLWF calculation. For example, [1,0,0] orientation refers to the donor atom that is displaced by a_0 in the x-direction with respect to the acceptor. This table references the additional data (red crosses) from Figure 3.

DAP	Orientation	Dipole moment (eÅ)
B-N m4 (diamond)	[1, 0, 0]	3.179
B-N m4 (diamond)	[-1, 0, 0]	3.502
B-N m4 (diamond)	[0, 1, 0]	3.179
B-N m4 (diamond)	[0, -1, 0]	3.502
B-N m4 (diamond)	[0, 0, 1]	3.179
B-N m4 (diamond)	[0, 0, -1]	4.036
B-N m5 (diamond)	[0.25, 0.75, 0.75]	3.687
B-N m5 (diamond)	[0.25, -0.75, -0.75]	4.117
B-N m5 (diamond)	[-0.25, 0.75, -0.75]	2.547
B-N m5 (diamond)	[-0.25, -0.75, 0.75]	5.175
B-N m5 (diamond)	[0.75, 0.25, 0.75]	2.746
B-N m5 (diamond)	[-0.75, 0.25, -0.75]	4.499
B-N m5 (diamond)	[-0.75, -0.25, 0.75]	5.175
B-N m5 (diamond)	[0.75, -0.25, -0.75]	4.117
B-N m5 (diamond)	[0.75, 0.75, 0.25]	2.746
B-N m5 (diamond)	[0.75, 0.75, 0.25]	2.746
B-N m5 (diamond)	[-0.75, -0.75, 0.25]	5.364
B-N m5 (diamond)	[0.75, -0.75, -0.25]	4.499
B-N m5 (diamond)	[-0.75, 0.75, -0.25]	5.364
B-N m4 (SiC)	[1, 0, 0]	3.279
B-N m4 (SiC)	[-1, 0, 0]	4.546
B-N m4 (SiC)	[0, 1, 0]	6.093
B-N m4 (SiC)	[0, -1, 0]	6.153
B-N m4 (SiC)	[0, 0, 1]	6.093
B-N m4 (SiC)	[0, 0, -1]	6.153
B-N m6 (SiC)	[-0.5, -0.5, -1]	6.483
B-N m6 (SiC)	[-0.5, -1, -0.5]	6.455
B-N m6 (SiC)	[-1, -0.5, -0.5]	5.274
B-N m6 (SiC)	[-0.5, -1, 0.5]	4.739
B-N m8 (SiC)	[1, 1, 0]	7.521
B-N m8 (SiC)	[-1, -1, 0]	7.420
B-N m8 (SiC)	[-1, 0, -1]	7.420
B-N m8 (SiC)	[0, -1, 1]	6.687
B-N m8 (SiC)	[0, -1, -1]	6.687

is significant especially for small pair separations [5–7], and approaches zero as the pair separation is increased. We find that the magnitudes for correction energies in the first few shells are in the expected range according to previous calculations and observations [7, 8]. The ZPL values obtained from constrained DFT already include the effects captured by $J(R_m)$. Therefore, in Figure 2, we subtract $J(R_m)$ from constrained DFT values to compensate for this effect.

We present in Supplementary Table 6 a summary of results obtained from Figure 2. The theoretical value for the slope $k_e e^2 \varepsilon_r^{-1} r_b^{-1}$ is 1.64 (0.78) eV for diamond (3C-SiC) when $\varepsilon_r = 5.7$ (9.72) and $r_b = 1.55$ (1.90) Å are used.

Supplementary Table 5: Methods for obtaining dipole moments. Comparison between the MLWF and the best fit methods for a select few B-N pairs in diamond. The dipole moments are reported in units of eÅ. The direction of the applied electric field is given in parenthesis in the first column. Only the component of the dipole moment parallel to the direction of the applied electric field is reported.

Shell # (dir)	Dipole moment (eÅ)	
	Best fit	MLWF
m5 (100)	-1.71	-1.72
m5 (010)	1.49	1.65
m5 (001)	3.13	3.36
m4 (100)	-3.19	-3.18
m6 (100)	1.53	1.76

Supplementary Table 6: Parameters obtained from the DAP model. A summary of results obtained from Figure 2. The slope and y-intercept values for the linear fit are reported in units of eV for both the PBE and the HSE functionals. The sum of the binding energies is determined by subtracting the y-intercept from the bandgap E_g

	B-N (diamond)		B-N (3C-SiC)		Al-N (3C-SiC)	
	PBE	HSE	PBE	HSE	PBE	HSE
slope	1.79	1.92	0.73	0.73	0.81	0.83
y-int	2.38	3.04	0.90	1.42	1.08	1.88
$E_D + E_A$	1.82	2.33	0.50	0.84	0.32	0.38

D. Huang-Rhys Factors & Electron-Phonon Coupling

In Supplementary Table 3 we report the calculated effective ground and excited frequencies $\Omega_{\{e,g\}}$ and effective HR factors $S_{\{e,g\}}$. The mass-weighted distortion ΔQ and ZPL belonging to each shell are also included. The effective one-dimensional frequencies extracted from a parabola fit to the ground and excited state potential energy surfaces for the CC diagrams are reported as well. Supplementary Figure 2 is a visualization of the data presented in this table.

E. Analysis of dipole-dipole interaction strengths

The interaction strength between two electric dipoles is given by the formula

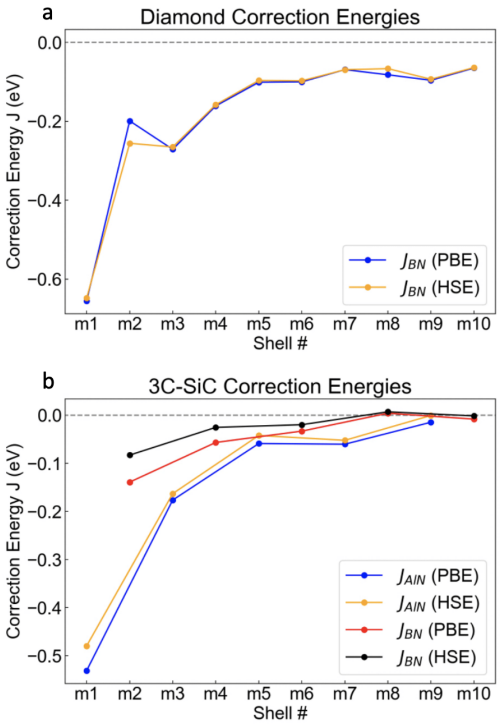

Supplementary Figure 1: Correction energies to the ZPLs of donor-acceptor pairs. $J(R_m)$ correction energies are presented as a function of shell number in (a) diamond and (b) 3C-SiC.

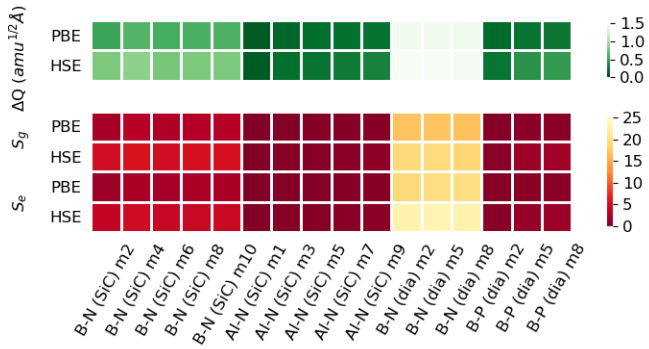

Supplementary Figure 2: Effective 1D model for donor-acceptor pairs. Visualization of calculated parameters from the effective one-dimensional model for DAP in 3C-SiC and diamond. Total mass-weighted distortion ΔQ are given as well as HR factors ($S_{\{e,g\}}$) in ground and excited states.

$$E_{dd} = \frac{p_i p_j}{4\pi\epsilon_0\varepsilon_r}\frac{1}{r_{ij}^3} f(\theta_1, \theta_2, \zeta) \tag{2}$$

where $f(\theta_1, \theta_2, \zeta)$ ranges between -2 and 2 and depends on the relative twist angles the dipoles make with respect to each other and relative to the axis connecting the two dipoles. We plot the interaction strength in MHz with respect to the distance between the two dipoles for several dipole strengths in Figure 1b. We take the value $f(\theta_1, \theta_2, \zeta)$ to be 1 and the dielectric constant as 9.72 for 3C-SiC. In the plot we include the spin-spin interaction resulting from two NV- centers interacting in diamond as well, with a different dielectric constant of 5.7. We assume an electric dipole moment of 5 eÅ for small shell numbers and 15 eÅ for relatively large shell numbers. Based on these parameters, it can be seen that an interaction strength of ∼100 MHz can easily be obtained from 100 nm away, depending on the strength of the dipoles involved. If even larger dipoles from larger shell numbers can be successfully controlled and manipulated, this interaction strength might be obtained from more than 100 nm away. Depending on the orientation of DAPs with respect to each other, this distance could be slightly different, in either direction.

F. Finite Size Effects

Shallow donors and acceptors, such as those studied in this paper, tend to form delocalized defect states that often give rise to supercell size effects in DFT simulations. Very often, large supercells consisting of more than a 1000 atoms might be necessary to accurately represent some of these delocalized defect states. Here we discuss a delicate balancing act between computational cost and accuracy when it comes to choosing the appropriate supercell size for our simulations. We report in Supplementary Table 8 the charge transition levels (CTL) of the shallow defects studied in this paper as a function of supercell size and their extrapolation to the dilute limit, using the PBE functional. While it is true that the delocalized orbitals belonging to these shallow defects are too large to fit even in 1000 atom supercells, we observe that increasing the supercell size from 512 atoms to 1000 atoms results in changes for the CTL by less than 0.05 eV in all cases. Given this small quantitative difference, we consider it appropriate to use 512 atom supercells for this study and think that using a 1000 atom supercell would not significantly impact the overall conclusions of this paper.

G. Experimental Investigations

Samples were placed in a Montana S200 onto a fixed copper post. All samples were addressed with a 0.5 NA Mitutoyo G Plan Apo 50X objective. Photoluminescence was generated with a Thorlabs L405P150 operating at 130 mW and directed to the sample with a dichroic mirror (Thorlabs DMPL425L). Spectra was focused directly into the spectrometer with an achromatic lens (Thorlabs AC-508-300-A-ML). Excess laser light was blocked from the spectrometer with two filters: Semrock BLP01-405R-

Supplementary Table 7: Details of sample preparation. The details for sample preparation are given below for the eleven diamond samples. Implantation type, concentration and annealing conditions are given for each sample.

Sample	Type	Concentration [N/B] (ppm)	Incorporation method [N/B]	Annealing
1	HPHT	700/0.1	Innate/Ion Implantation	800C 5 hours Ar/H_2
2	HPHT	700/1.0	Innate/Ion Implantation	800C 5 hours Ar/H_2
3	HPHT	700/10	Innate/Ion Implantation	800C 5 hours Ar/H_2
4	HPHT	700/100	Innate/Ion Implantation	800C 5 hours Ar/H_2
5	CVD: Optical	0.6/10	Innate/Ion Implantation	800C 5 hours Ar/H_2
6	CVD: Optical	10/0.05	Ion Implantation/Innate	800C 5 hours Ar/H_2
7	CVD: Optical	10/10	Ion Implantation	800C 5 hours Ar/H_2
8	CVD: Optical	0.6/0.5	Innate	–
9	CVD: Electronic	1.0/1.0	Ion Implantation	800C 5 hours Ar/H_2
10	CVD: Electronic	1.0/1.0	Ion Implantation	400C 8 hours, 800C 8 hours, 1200C 2 hours Ar/H_2 Diacid boil
11	CVD: Electronic	10/10	Ion Implantation	400C 8 hours, 800C 8 hours, 1200C 2 hours Ar/H_2 Diacid boil

Supplementary Table 8: Finite size effects. Charge transition levels (CTL) of shallow defects in diamond and 3C-SiC reported in eV as a function of supercell size, and their extrapolation to the dilute limit. Donors and acceptors CTL are reported with respect to their respective band edges. The extrapolation to the dilute limit was done using a linear fit using $1/L^3$ as the argument, in other words, using the volume of the supercell.

	Supercell size				
Defect	64	216	512	1000	∞
B_C (diamond)	0.703	0.438	0.347	0.329	0.306
P_C (diamond)	0.888	0.566	0.455	0.456	0.415
N_C (3C-SiC)	0.468	0.240	0.158	0.122	0.113
Al_{Si}(3C-SiC)	0.318	0.202	0.169	0.141	0.141

25 and Newport FSR GG420. Our spectrometer is a Princeton Instruments HRS-500, with a PIXIS 400 CCD camera and a 1200 g mm^{-1} grating blazed at 750nm. The details about sample preparation details are included in Supplementary Table 7

[1] P. Deák, B. Aradi, M. Kaviani, T. Frauenheim, and A. Gali, Formation of NV centers in diamond: A theoretical study based on calculated transitions and migration of nitrogen and vacancy related defects, Phys. Rev. B **89**, 075203 (2014).

[2] K. Czelej, P. Śpiewak, and K. Kurzydłowski, Electronic structure of substitutionally doped diamond: Spin-polarized, hybrid density functional theory analysis, Diam. Relat. Mater. **75**, 146 (2017).

[3] H. Kim, A. K. Ramdas, and S. Rodriguez, Spontaneous symmetry breaking of acceptors in 'blue' diamonds, Phys. Rev. Lett. **83**, 4140 (1999).

[4] J. Davidsson et al., First principles predictions of magneto-optical data for semiconductor point defect identification: the case of divacancy defects in 4H–SiC, New J. Phys. **20**, 023035 (2018).

[5] D. G. Thomas, M. Gershenzon, and F. A. Trumbore, Pair spectra and 'edge' emission in gallium phosphide, Phys. Rev. **133**, 1A A269 (1964).

[6] W. Schmid, U. Nieper, and J. Weber, Donor-acceptor pair spectra in Si:In LPE-layers, Solid State Commun. **45**, 1007 (1983).

[7] B. Dischler et al., Resolved donor-acceptor pair-recombination lines in diamond luminescence, Phys. Rev. B **49**, 1685 (1994).

[8] F. E. Williams, Theory of the energy levels of donor-acceptor pairs, J. Phys. Chem. Lett. **12**, 265 (1960).